LETTERS
PUBLISHED ONLINE: 4 JANUARY 2016 | DOI: 10.1038/NPHYS3609
nature physics

Selective scattering between Floquet–Bloch and Volkov states in a topological insulator

Fahad Mahmood, Ching-Kit Chan, Zhanybek Alpichshev, Dillon Gardner, Young Lee, Patrick A. Lee and Nuh Gedik*

The coherent optical manipulation of solids is emerging as a promising way to engineer novel quantum states of matter[1–5]. The strong time-periodic potential of intense laser light can be used to generate hybrid photon–electron states. Interaction of light with Bloch states leads to Floquet–Bloch states, which are essential in realizing new photo-induced quantum phases[6–8]. Similarly, dressing of free-electron states near the surface of a solid generates Volkov states, which are used to study nonlinear optics in atoms and semiconductors[9]. The interaction of these two dynamic states with each other remains an open experimental problem. Here we use time- and angle-resolved photoemission spectroscopy (Tr-ARPES) to selectively study the transition between these two states on the surface of the topological insulator Bi_2Se_3. We find that the coupling between the two strongly depends on the electron momentum, providing a route to enhance or inhibit it. Moreover, by controlling the light polarization we can negate Volkov states to generate pure Floquet–Bloch states. This work establishes a systematic path for the coherent manipulation of solids via light–matter interaction.

The manipulation of solids using ultrafast optical pulses has opened up a new paradigm in condensed matter physics by allowing the study of emergent physical properties that are otherwise inaccessible in equilibrium[1,2,10]. An important example is provided by the Floquet–Bloch states[11], which emerge in solids owing to a coherent interaction between Bloch states inside the solid and a periodic driving potential. This is a consequence of the Floquet theorem[12], which states that a Hamiltonian periodic in time with period T has eigenstates that are evenly spaced by the drive energy $(2\pi/T)$. Floquet–Bloch states have generated a lot of interest recently both for realizing exotic states of matter such as a Floquet Chern insulator[7], as well as understanding non-equilibrium periodic thermodynamics[13,14]. Experimental observation of these states requires the measurement of the transient electronic band structure of a crystal as it is perturbed by light. As has recently been demonstrated[15] in the topological insulator Bi_2Se_3, time- and angle-resolved photoemission spectroscopy (Tr-ARPES) is a key tool that can achieve this. Characteristic signatures of Floquet–Bloch states in the Tr-ARPES spectra include replicas of the original band structure that are separated by the driving photon energy[15].

In addition to Floquet–Bloch states, light can also generate other coherent phenomena in solids[16–18]. In particular, it can dress free-electron states near the surface of a solid (Fig. 1a), as the surface can provide the momentum conservation necessary for a photon to interact with a free electron. This dressing was first observed in time-resolved photoemission experiments[17] and has subsequently been referred to as laser-assisted photoemission (LAPE). LAPE is typically understood[19–21] by invoking the Volkov solution, which is an exact solution of the time-dependent Schrodinger equation for a free electron interacting with a plane electromagnetic wave[22]. LAPE bands can thus be thought of as Volkov states in vacuum that electrons can transition into from initial Bloch states inside the solid. In a Tr-ARPES experiment, the final state of photoemission is typically free-electron-like, and dressing of these final states generates Volkov states that, similar to Floquet–Bloch states, appear in the spectra as band replicas separated by the driving photon energy. In this work we will refer to the dressing of initial states as Floquet–Bloch states and the dressing of the final states as Volkov states.

Both these dressed states cause band replicas in the Tr-ARPES spectra which appear at the same energy and momentum regardless of whether they originate from Floquet–Bloch or Volkov states, making it difficult to distinguish between them. Moreover, owing to the coherent nature of both processes, electrons can scatter directly from Floquet–Bloch states into Volkov states[23] (Fig. 1a). To study the various exotic affects predicted by Floquet theory on solid-state systems, it is important to experimentally characterize and separate out Floquet–Bloch and Volkov states in a controlled way. Furthermore, the interaction between Volkov and Floquet–Bloch states can provide novel insights into using semiconductors for nonlinear optics[9].

In this Letter, we use Tr-ARPES on Bi_2Se_3 with mid-infrared excitation pulses to selectively study transitions between Floquet–Bloch and Volkov states. We find that interference between Floquet–Bloch and Volkov states must be taken into account to explain the intensity and the angular dependence of the dressed states in the Tr-ARPES spectra. Moreover, by controlling the polarization of the dressing field we can enhance or inhibit this interference. We also find that the observed hybridization between different dressed sidebands is independent of Volkov states, and thus is a key signature of Floquet–Bloch states emerging in a solid.

Tr-ARPES measurements were performed using mid-infrared 160 meV pulses as the pump and 6.3 eV pulses as the probe. A time-of-flight analyser is used to simultaneously acquire the complete transient band structure of Bi_2Se_3 without rotating the sample or the detector[24]. The mid-infrared pump beam was incident on the sample at an angle of $\sim 45^\circ$ and its polarization was set to either P or S with respect to the incidence plane (Fig. 1b). The P-polarized pump includes an out-of plane electric field component, whereas the S-polarized pump is purely in plane. Figure 1c shows the Tr-ARPES spectra using the P-polarized pump on Bi_2Se_3 at various delay times between the pump and probe. Replicas of the original Dirac cone appear when the pump and probe pulse overlap in time. These replicas are electron states dressed by the intense

Department of Physics, Massachusetts Institute of Technology, Cambridge, Massachusetts 02139, USA. *e-mail: gedik@mit.edu

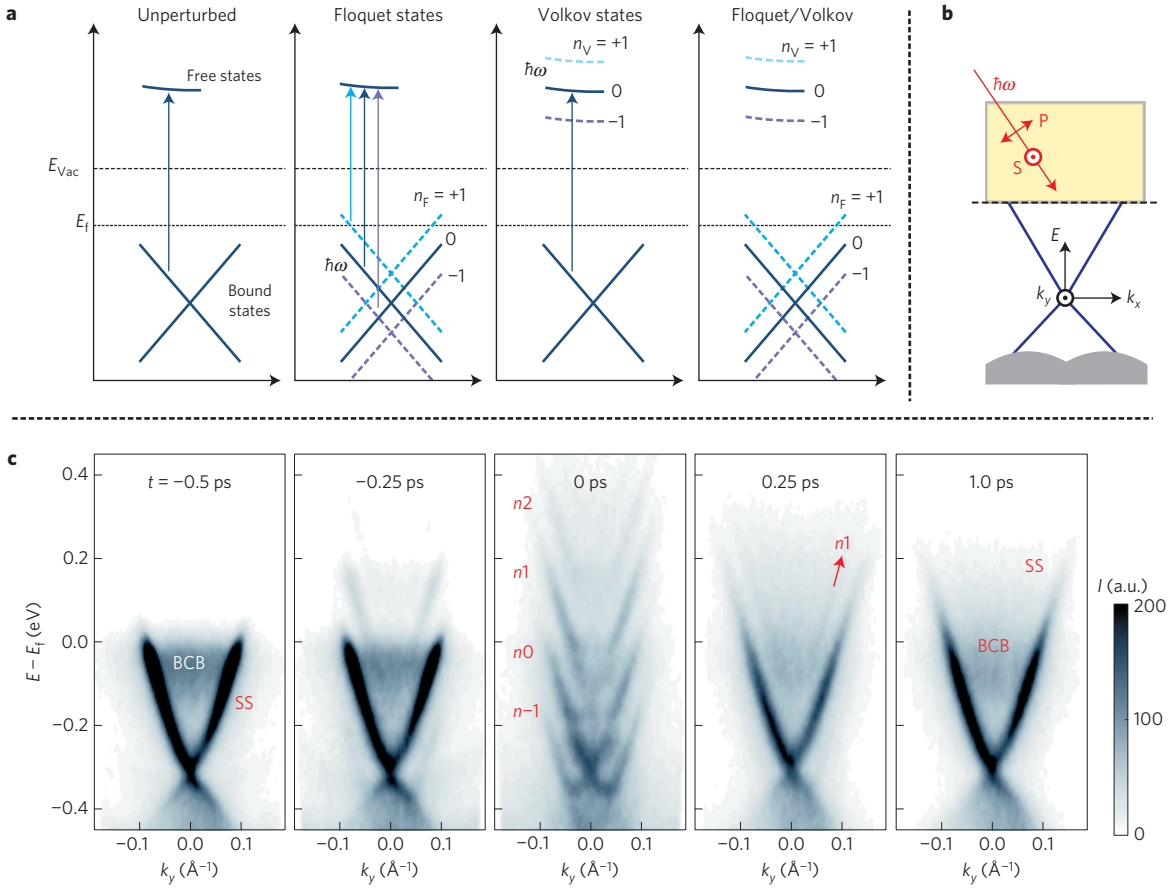

Figure 1 | Dressed electron states in the Tr-ARPES spectra of a topological insulator and experimental geometry. a, Schematic illustrating the various transitions in a Tr-ARPES experiment. In the unperturbed case or before time zero, electrons transition from bound states to free-electron-like states. Dressing of the bound states results in Floquet states (n_F) separated by the drive photon energy ω, whereas dressing of the free-electron-like states results in Volkov states (n_V). If both the initial and final states are dressed (rightmost panel), the nth-order sideband in the Tr-ARPES spectra is given by all transitions such that $n = n_F + n_V$. **b**, Experimental geometry of the Tr-ARPES set-up. The pump light is incident onto the sample at an angle of ∼45°. The pump is linearly polarized with the P-polarization having an out-of-plane component and an in-plane component along the k_x direction, whereas the S-polarization is purely in-plane along the k_y direction. **c**, Tr-ARPES ($E - E_f$ versus k_y) spectra on Bi_2Se_3 using the P-polarized pump at various delay times between the pump and the probe. BCB refers to the bulk conduction band and SS refers to the topological surface state. The nth-order sidebands are indicated in the spectra at $t = 0$.

pump pulse. The intensity of these sidebands is maximized at $t = 0$, which refers to the maximum E-field of the pump beam coinciding with the maximum E-field of the probe. Once the dressing field of the pump pulse disappears ($t > 500$ fs), the sidebands disappear, leaving a heated Dirac cone. The dynamics of this non-equilibrium heated distribution of electrons has been discussed in a number of Tr-ARPES experiments[25–28]. Here we will focus on the Tr-ARPES spectra taken at $t = 0$ to ascertain the relative contribution of Floquet–Bloch and Volkov states.

To disentangle the two, we study the Tr-ARPES spectra at $t = 0$ along various directions of the electron momentum. Figure 2a and b show the spectra along the k_x and the k_y directions respectively, taken with the linear P-polarized pump with an in-plane electric field component along k_x (Fig. 1b). Two observations are apparent: avoided crossing gaps along k_y (Fig. 2b, red arrows) but not along k_x, and asymmetry in the intensity of Floquet sidebands about $k_x = 0$. The first observation is consistent with Floquet–Bloch theory on Dirac systems[29–32]. As the pump E-field is along the x-direction, the perturbing Hamiltonian commutes with the Dirac Hamiltonian corresponding to electrons with momentum along k_x. This leads to a trivial crossing between sidebands along k_x, which thus remains gapless. However, along k_y, the direction perpendicular to the E-field, avoided crossing gaps open up. The gap (2Δ) at the crossing between the zeroth- and first-order sideband is predicted[32] to scale linearly with the electric field amplitude (E_0), and thus $2\Delta \propto \sqrt{P}$, where P is the applied average pump power. By plotting the measured value of the gap as a function of the pump power on a log–log plot (Fig. 2c), we find that 2Δ indeed scales as the square root of the pump power. This observation unequivocally establishes the transient generation of Floquet–Bloch states.

The second observation of asymmetry in the intensity of the sidebands allows us to establish scattering between Floquet–Bloch and Volkov states. As seen in Fig. 2a, the first-order sideband ($n1$) is not an exact replica of the original band ($n0$). Rather, the replication of the Dirac cone is asymmetric between the $+k_x$ and $-k_x$ directions. It is important to distinguish this from the asymmetry in the intensity of the Dirac cone that arises in the unperturbed ARPES spectra. Owing to the coupling of the photoemitting 6 eV probe beam to the spin texture of the Dirac cone, there is a natural asymmetry between the $+k_x$ and $-k_x$ directions because the incident plane of the photoemitting probe is along the k_x direction. This matrix element (spin–probe) effect has been well understood in other ARPES measurements on similar systems[24]. Here, we will study the additional asymmetry that is present in the replica of the original Dirac cone. This asymmetry is more evident in constant energy cuts separated by the driving photon energy

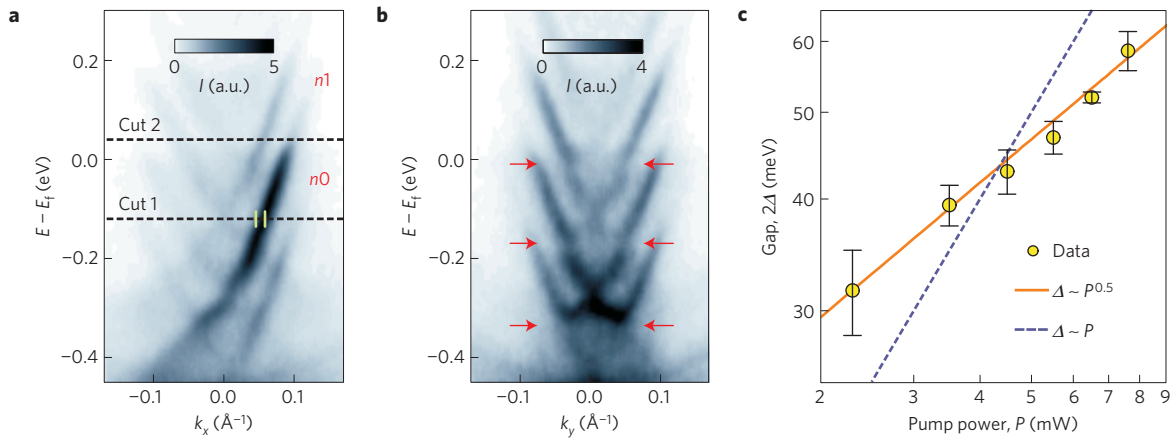

Figure 2 | Tr-ARPES spectra of Bi_2Se_3 at $t=0$ for P-polarized pump. a,**b**, Energy (E) relative to the Fermi level (E_f) versus momentum along the k_x direction (**a**) and along the k_y direction (**b**). Red arrows indicate the avoided crossing gaps. Green lines in **a** indicate the momentum window over which the data is integrated to obtain the angular distribution of I_1/I_0 in Fig. 3d. **c**, Avoided crossing gap (2Δ) as a function of incident pump power (P) on a log–log plot. The gap at each pump power is obtained by fitting the energy distribution curves in the ARPES spectra with a pair of Lorentzians (Supplementary Text). Error bars represent the 95% confidence interval (2 s.d.) in extracting the gap from the fitting parameters. Power laws ($\Delta \sim P^{\eta}$) with $\eta=0.5$ (orange trace) and $\eta=1$ (blue trace) are plotted as well to determine the analytical behaviour of 2Δ with P.

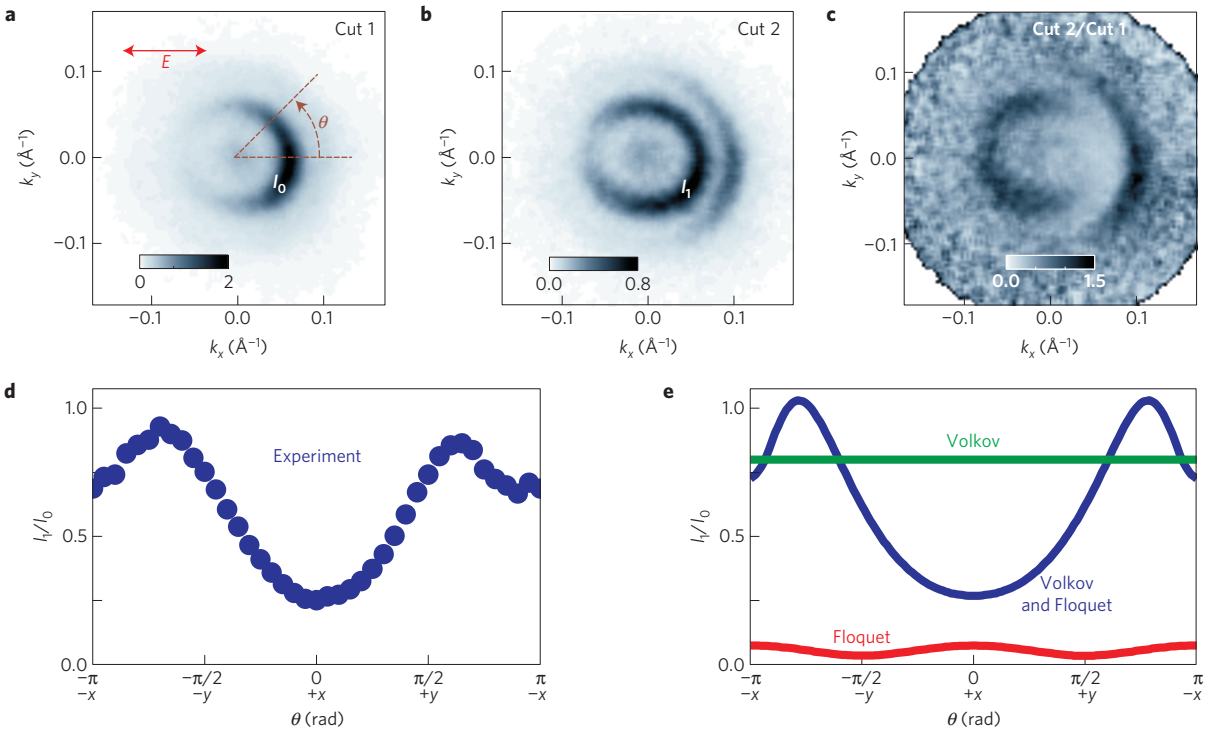

Figure 3 | Asymmetry in the Tr-ARPES spectra. a, Constant energy cut at $E-E_f=-0.12$ eV (that is, along dashed line 'Cut 1' in Fig. 2a). The electric field (**E**) is along the k_x direction (red arrow). I_0 indicates the surface state contour for the zeroth-order band (that is, the original Dirac cone). **b**, Constant energy cut at $E-E_f=0.04$ eV (that is, along dashed line 'Cut 2' in Fig. 2a). The two constant energy cuts are separated in energy by the driving pump energy of 160 meV. I_1 indicates the surface state contour for the first-order side band. **c**, The constant energy cut in **b** is divided by the cut in **a** and the result is shown as a colour plot. **d**, Distribution of I_1/I_0 as a function of angle (θ) measured from the $+k_x$ direction. The distribution is obtained by radially integrating the surface state contours in **a** and **b** over a 'k' space window of width ~0.013 Å^{-1}. The momentum window is centred at $k=0.05$ Å^{-1} and is indicated by green lines on Fig. 2a. **e**, Calculated angular distribution of I_1/I_0 for the P-polarized pump at different values of the LAPE parameter (α) and the Floquet parameter (β). Red trace: $\alpha=0$ and $\beta=0.5$. Green trace: $\alpha=1.38$ and $\beta=0$. Blue trace: $\alpha=1.38$ and $\beta=0.5$.

(Fig. 3a,b). To minimize the effects of spin texture as well as detector nonlinearities, we divide these constant energy cuts (I_1/I_0) and plot the result in Fig. 3c. If the $n1$ sideband were an exact replica of the $n0$ sideband, then I_1/I_0 would be constant as a function of the electron momentum. However, as can be seen in Fig. 3c,d, I_1/I_0 is stronger along the $-k_x$ direction than along the $+k_x$ direction, indicating that the dressed bands strongly depend on the direction of the electron momentum.

To explain this, we model our Tr-ARPES spectra by including the effects of both Floquet–Bloch and Volkov states. We start with

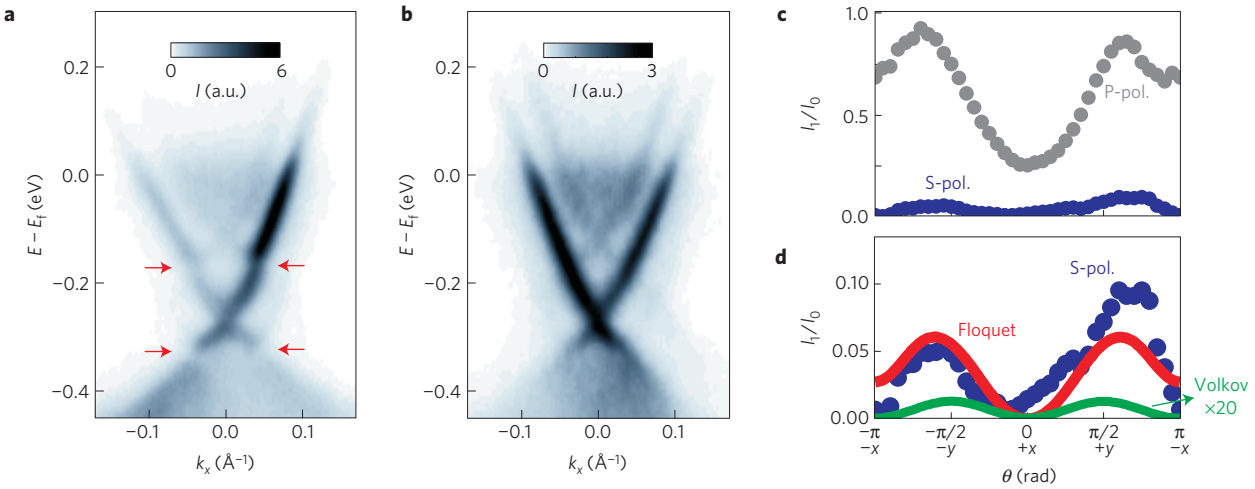

Figure 4 | Tr-ARPES spectra at $t=0$ for S-polarized pump. a,**b**, Energy (E) relative to the Fermi level (E_f) versus momentum along the k_x direction (**a**) and along the k_y direction (**b**). Red arrows indicate the avoided crossing gaps. **c**, Ratio of the first-order side band intensity I_1 to the zeroth-order intensity I_0 as a function of angle (θ) measured from the $+k_x$ direction, for both P and S-polarized pumps. I_1/I_0 for the S-polarized pump is obtained in the same way as that for the P-polarized pump (Fig. 3). **d**, I_1/I_0 for the S-polarized pump (blue trace) along with the calculated angular distribution of I_1/I_0 for the S-polarized pump using: $\alpha=0$ and $\beta=0.5$ (red trace). The discrepancy between the calculated (red trace) and measured (blue dots) values is probably due to instrument limitations in measuring the extremely small intensity of the $n1$ sideband for the S-polarized pump. Green trace represents the calculated I_1/I_0 for Case 1 with $\alpha=0.05$ and $\beta=0$. These values correspond to Volkov states being generated by the in-plane electric field only (Supplementary Information). Note: I_1/I_0 for the green trace has been multiplied by 20 for better visual representation on this axis scale.

the Dirac Hamiltonian describing the surface states of a topological insulator (Supplementary Information). The mid-infrared laser pump is introduced through the Peierls' substitution—that is, $v_f\mathbf{k}\rightarrow v_f\mathbf{k}+ev_f\mathbf{A}$, where $\mathbf{A}$ is the vector potential of the pump light and v_f is the Fermi velocity. The dimensionless parameter $\beta=ev_fA/\omega$ characterizes the strength of the Floquet interaction, where ω is the frequency of the mid-infrared laser pump. The resulting Tr-ARPES intensity can be obtained[33] by using the non-equilibrium two-time correlation function of the driven electrons (Supplementary Information). Without including the effect of Volkov states (LAPE), this results in the following expression for the photoemitted intensity for the case of electron momentum along the linearly polarized pump direction (that is, along k_x):

$$I(k_x,E)\propto\sum_n\{\delta_{E,\hbar v_f k_x+n\hbar\omega}+\delta_{E,-\hbar v_f k_x+n\hbar\omega}\}J_n(\beta)^2 \qquad (1)$$

where J_n are Bessel functions of the first kind. Therefore, the nth Floquet–Bloch sideband has an intensity $\sim J_n(\beta)^2$ and is symmetric for $\pm k_x$. The situation becomes different when the effect of Volkov states is included. The corresponding Hamiltonian is $H_{\mathrm{LAPE}}=\hbar e\mathbf{v}_0\cdot\mathbf{A}$, where $\mathbf{v}_0$ is the free photoelectron velocity, obtained by conserving energy and in-plane momentum in the photoemission process. The dimensionless parameter $\alpha=ev_0A/\omega$ characterizes the interaction strength between light and the final states of photoemission. The photoemitted intensity (along k_x) now becomes (Supplementary Information):

$$I(k_x,E)\propto\sum_n[\delta_{E,\hbar v_f k_x+n\hbar\omega}J_n(\beta-\alpha)^2+\delta_{E,-\hbar v_f k_x+n\hbar\omega}J_n(\beta+\alpha)^2] \quad (2)$$

The dependence on both α and β is due to the interference between Floquet–Bloch and Volkov states. The observed nth-order sideband is now a combination of different Fourier pairs of Floquet–Bloch (n_F) and Volkov (n_V) modes such that $n_F+n_V=n$ (Fig. 1a). To explain the data fully, we have also included the spin–probe effect that describes the coupling of the photoemitting probe to the spin texture of the Dirac cone (Supplementary Information).

Figure 3e shows the results of this calculation for three different cases: Case 1, $\alpha=0$ and $\beta=0.5$ (Floquet only); Case 2, $\alpha=1.38$ and $\beta=0$ (Volkov only); and Case 3 $\alpha=1.38$ and $\beta=0.5$ (Floquet and Volkov). The non-zero values used for α and β agree fairly well with the measured experimental parameters (v_f, v_0, A and ω) of the set-up (Methods). In Case 1 (red trace) electrons scatter from dressed states in the solid (Floquet–Bloch) into unperturbed free-electron states. The two-fold rotational symmetry is understood by noting that the electrons scatter preferentially when their momentum is along the direction of the light polarization (in this case along k_x). Case 2 (green trace) refers to the situation when only the final states are dressed (Volkov). Here it is important to note that in the photoemission process only the in-plane momentum is conserved, whereas the electrons acquire a large out-of-plane momentum (k_z) due to the excess photon energy. Because the pump pulse is P-polarized, the electric field in the z-direction strongly couples to free-electron states with a large v_z, leading to a dressing of these final states that predominately depends on the out-of-plane momentum. The intensity of the sidebands is thus isotropic as a function of in-plane momentum (green trace).

Case 3 (blue trace) includes the dressing of both the initial and final states and, as can be seen, this trace closely matches the observed angular dependence in the intensity of the first-order sideband (Fig. 3d). The calculation also captures the strong asymmetry in I_1/I_0 between $+k_x$ and $-k_x$, which would not be present for pure Floquet–Bloch (Case 1) or pure Volkov states (Case 2). There is also good agreement between the experimental and calculated values of I_2/I_0 for the same values of α and β as used for I_1/I_0 (Supplementary Information). These results not only imply the presence of both Floquet–Bloch and Volkov states, but also point to selective transitions between the two. For example, as the electron momentum is varied between $-k_x$ and $+k_x$, there is an increase and then decrease in the scattering intensity as recorded by Tr-ARPES. As discussed above, equation (2) implies that for electron momentum along the light polarization direction (that is, along k_x), the photoemitted intensity can be written as $\propto J_n(\beta\mp\alpha)^2$ for $\pm k_x$. Thus, by varying the electron momentum, we can control the scattering between Floquet–Bloch and Volkov states. These selective transitions are a

direct consequence of Volkov states being generated primarily due to the out-of-plane E-field for the P-polarized pump.

The aforementioned result suggests a way to reduce the effect of Volkov states: eliminating the out-of-plane electric field. This can be achieved by perturbing the system with S-polarized light instead. Figure 4a and b show the Tr-ARPES spectra at $t = 0$ along the k_x and k_y directions respectively, taken with the S-polarized pump oriented along the k_y direction. Similar to the P-polarized pump, avoided crossing gaps are apparent (red arrows, Fig. 4a). However, the gaps are now observed along the k_x direction, but not along the k_y direction. This is again consistent with Floquet–Bloch theory on Dirac electrons, because the avoided crossing gaps are along the momentum direction (k_x) perpendicular to the direction of the E-field (k_y). We can also notice a significant decrease in the intensity of the sidebands despite using a similar intensity for the pump. We again take the ratio of the intensities of the first- and zeroth-order sidebands (I_1/I_0) and plot it as a function of the electron momentum direction (Fig. 4c). This ratio is almost ten times less than what is observed for the P-polarized pump. We attribute this to a minimization of Volkov states, which is confirmed by numerically calculating the sideband intensities case for the presence of Floquet–Bloch states only (Case 1; $\alpha = 0$ & $\beta = 0.5$) using the S-polarized pump. As can be seen (Fig. 4d), the calculation agrees fairly well with the observed angular dependence of I_1/I_0. Thus, perturbing the system with the S-polarized mid-infrared pump results in the generation and observation of pure Floquet–Bloch states. Moreover, by controlling the light polarization, we can enhance or completely inhibit the transition between Floquet–Bloch and Volkov states.

The systematic characterization of these electron–photon hybrid states has important implications for the coherent manipulation of quantum states and various techniques used to investigate this phenomenon. Understanding the coupling of Floquet–Bloch states to other electronic states is crucial for engineering novel light-induced quantum phases of matter. Furthermore, the observed interference between initial and final dressed states extends beyond Tr-ARPES; it will also manifest in other experimental techniques such as tunnelling spectroscopy of light-dressed electronic systems.

Methods

Methods and any associated references are available in the online version of the paper.

Received 19 July 2015; accepted 19 November 2015; published online 4 January 2016

References

1. Hu, W. *et al.* Optically enhanced coherent transport in $YBa_2Cu_3O_{6.5}$ by ultrafast redistribution of interlayer coupling. *Nature Mater.* **13,** 705–711 (2014).
2. Matsunaga, R. *et al.* Light-induced collective pseudospin precession resonating with Higgs mode in a superconductor. *Science* **345,** 1145–1149 (2014).
3. Kirilyuk, A., Kimel, A. V. & Rasing, T. Ultrafast optical manipulation of magnetic order. *Rev. Mod. Phys.* **82,** 2731–2784 (2010).
4. Caviglia, A. D. *et al.* Ultrafast strain engineering in complex oxide heterostructures. *Phys. Rev. Lett.* **108,** 136801 (2012).
5. Mentink, J. H., Balzer, K. & Eckstein, M. Ultrafast and reversible control of the exchange interaction in Mott insulators. *Nature Commun.* **6,** 6708 (2015).
6. Lindner, N. H., Refael, G. & Galitski, V. Floquet topological insulator in semiconductor quantum wells. *Nature Phys.* **7,** 490–495 (2011).
7. Grushin, A. G., Gómez-León, Á. & Neupert, T. Floquet fractional Chern insulators. *Phys. Rev. Lett.* **112,** 156801 (2014).
8. Kitagawa, T., Oka, T., Brataas, A., Fu, L. & Demler, E. Transport properties of nonequilibrium systems under the application of light: Photoinduced quantum Hall insulators without Landau levels. *Phys. Rev. B* **84,** 235108 (2011).
9. Wegener, M. *Extreme Non-linear Optics* (Springer, 2005).
10. Stojchevska, L. *et al.* Ultrafast switching to a stable hidden quantum state in an electronic crystal. *Science* **344,** 177–180 (2014).
11. Faisal, F. H. M. & Kamiński, J. Z. Floquet–Bloch theory of high-harmonic generation in periodic structures. *Phys. Rev. A* **56,** 748–762 (1997).
12. Galitski, V. M., Goreslavskii, S. P. & Elesin, V. F. Electric and magnetic properties of a semiconductor in the field of a strong electromagnetic wave. *J. Exp. Theor. Phys.* **30,** 117–122 (1970).
13. Kohn, W. Periodic thermodynamics. *J. Stat. Phys.* **103,** 417–423 (2001).
14. Eisert, J., Friesdorf, M. & Gogolin, C. Quantum many-body systems out of equilibrium. *Nature Phys.* **11,** 124–130 (2015).
15. Wang, Y. H., Steinberg, H., Jarillo-Herrero, P. & Gedik, N. Observation of Floquet–Bloch states on the surface of a topological insulator. *Science* **342,** 453–457 (2013).
16. Schmitt, F. *et al.* Transient electronic structure and melting of a charge density wave in $TbTe_3$. *Science* **321,** 1649–1652 (2008).
17. Saathoff, G., Miaja-Avila, L., Aeschlimann, M., Murnane, M. M. & Kapteyn, H. C. Laser-assisted photoemission from surfaces. *Phys. Rev. A* **77,** 022903 (2008).
18. Miaja-Avila, L. *et al.* Ultrafast studies of electronic processes at surfaces using the laser-assisted photoelectric effect with long-wavelength dressing light. *Phys. Rev. A* **79,** 030901 (2009).
19. Glover, T. E., Schoenlein, R. W., Chin, A. H. & Shank, C. V. Observation of laser assisted photoelectric effect and femtosecond high order harmonic radiation. *Phys. Rev. Lett.* **76,** 2468–2471 (1996).
20. Madsen, L. B. Strong-field approximation in laser-assisted dynamics. *Am. J. Phys.* **73,** 57–62 (2005).
21. Baggesen, J. C. & Madsen, L. B. Theory for time-resolved measurements of laser-induced electron emission from metal surfaces. *Phys. Rev. A* **78,** 032903 (2008).
22. Joachain, C. J., Kylstra, N. J. & Potvliege, R. M. *Atoms in Intense Laser Fields* (Cambridge Univ. Press, 2014).
23. Park, S. T. Interference in Floquet–Volkov transitions. *Phys. Rev. A* **90,** 013420 (2014).
24. Wang, Y. H. *et al.* Observation of a warped helical spin texture in Bi_2Se_3 from circular dichroism angle-resolved photoemission spectroscopy. *Phys. Rev. Lett.* **107,** 207602 (2011).
25. Wang, Y. H. *et al.* Measurement of intrinsic Dirac fermion cooling on the surface of the topological insulator Bi_2Se_3 using time-resolved and angle-resolved photoemission spectroscopy. *Phys. Rev. Lett.* **109,** 127401 (2012).
26. Sobota, J. A. *et al.* Ultrafast optical excitation of a persistent surface-state population in the topological insulator Bi_2Se_3. *Phys. Rev. Lett.* **108,** 117403 (2012).
27. Hajlaoui, M. *et al.* Ultrafast surface carrier dynamics in the topological insulator Bi_2Te_3. *Nano Lett.* **12,** 3532–3536 (2012).
28. Hajlaoui, M. *et al.* Tuning a Schottky barrier in a photoexcited topological insulator with transient Dirac cone electron–hole asymmetry. *Nature Commun.* **5,** 3003 (2014).
29. Syzranov, S. V., Fistul, M. V. & Efetov, K. B. Effect of radiation on transport in graphene. *Phys. Rev. B* **78,** 045407 (2008).
30. Oka, T. & Aoki, H. Photovoltaic Hall effect in graphene. *Phys. Rev. B* **79,** 081406 (2009).
31. Zhou, Y. & Wu, M. W. Optical response of graphene under intense terahertz fields. *Phys. Rev. B* **83,** 245436 (2011).
32. Fregoso, B. M., Wang, Y. H., Gedik, N. & Galitski, V. Driven electronic states at the surface of a topological insulator. *Phys. Rev. B* **88,** 155129 (2013).
33. Freericks, J. K., Krishnamurthy, H. R. & Pruschke, T. Theoretical description of time-resolved photoemission spectroscopy: Application to pump–probe experiments. *Phys. Rev. Lett.* **102,** 136401 (2009).

Acknowledgements

The authors would like to thank C. Lee for useful discussions. This work is supported by US Department of Energy (DOE), Basic Energy Sciences, Division of Materials Sciences and Engineering (experimental set-up, data acquisition and theory), Army Research Office (electron spectrometer) and by the Gordon and Betty Moore Foundation's EPiQS Initiative through Grant GBMF4540 (data analysis).

Author contributions

F.M. performed the experiments and the data analysis. C.-K.C. developed the theoretical methods and the numerical simulations. F.M. and C.-K.C. wrote the initial drafts of the main text and the Supplementary Information, respectively. N.G., P.A.L. and Z.A. gave crucial inputs to the writing of the manuscript. The samples were synthesized by D.G. and Y.L. This project was supervised by N.G.

Additional information

Supplementary information is available in the online version of the paper. Reprints and permissions information is available online at www.nature.com/reprints. Correspondence and requests for materials should be addressed to N.G.

Competing financial interests

The authors declare no competing financial interests.

Methods

Single crystals of Bi_2Se_3 were cleaved under ultrahigh vacuum ($<1 \times 10^{-10}$ torr) at a temperature of 30 K. Tr-ARPES measurements were performed using a pump–probe scheme. An optical parametric amplifier (OPA) is used to generate the mid-infrared 160 meV pump pulses. The probe beam consists of 6.3 eV pulses generated by frequency-quadrupling laser pulses from a Ti:sapphire amplifier. A time-of-flight analyser is used to simultaneously collect the complete band structure without rotating the sample or the detector.

The dimensionless parameter $\alpha = ev_0A_0/\omega$ characterizes the interaction strength between light and final states of photoemission (Volkov), whereas $\beta = ev_fA_i/\omega$ characterizes the strength of the Floquet interaction. Here $A_{0,i} = E_{0,i}/\omega$, where $E_{0,i}$ is the electric field amplitude along a particular electron velocity direction. For the Floquet interaction (β), the relevant velocity is the Fermi velocity of the surface state electrons. As this velocity is purely in place, the relevant electric field (E_i) is the one parallel to the sample surface. We used a pump power of 11.5 mW, which corresponds to an in-plane electric field of $E_i = 3.3 \times 10^7$ V m^{-1} (see detailed explanation of estimate in the Supplementary Section of ref. 15). Taking $v_f = 5 \times 10^5$ m s^{-1}, we obtain $\beta = 0.42$.

For the Volkov interaction (α), we determine the electron velocity in the final state of photoemission. As the in-plane momentum is conserved in the photoemission process and given that the final state is free-electron-like, we determine the in-plane velocity, $v_\parallel = 5.79 \times 10^4$ m s^{-1} for momentum $k = 0.05$ Å^{-1}. By conserving energy, this gives the out-of-plane electron velocity, $v_z = 4.55 \times 10^5$ m s^{-1}. As $v_z \gg v_\parallel$, the relevant velocity for the Volkov interaction is v_z and the relevant electric field (E_0) is the out-of-plane component of the electric field outside the sample surface. Using the Fresnel equations, we obtain $E_0 = 11.6 \times 10^7$ V m^{-1}, and thus $\alpha \sim 1.36$–1.4. The values of $\alpha = 1.38$ and $\beta = 0.5$ used in the calculations of sideband intensities are determined by fitting the observed intensities in the Tr-ARPES spectrum to the theoretically calculated intensities. Given the large uncertainty in determining the exact electric field at the sample surface, these values are consistent with the values calculated in this section.